Electronic Supplementary Material (ESI) for ChemComm.

Electronic Supplementary Information

Enhanced photocatalytic activity of gold nanoparticles driven by supramolecular host-guest chemistry

Marc Padilla, Francesca Peccati, José Luis Bourdelande, Xavier Solans-Monfort, Gonzalo Guirado, Mariona Sodupe* and Jordi Hernando*

Contents

I. MATERIALS AND METHODS

Materials

Reactants were purchased from Sigma-Aldrich and used without further purification. β-cyclodextrin was oven-dried for 12 h prior to its use. Solvents were purchased from Scharlab and use as received unless indicated. Thin layer chromatography was conducted over 0.25-cm thick *Alugram* foil *Sil G/UV*$_{254}$. Flash column chromatography was performed using Silica 60 (0.04 – 0.06 mm) 230-240 mesh as stationary phase. Dialysis processes were done using Cellu Step T1 cellullose membranes (3500 Da).

Characterization techniques

^{1}H-NMR and ^{13}C-NMR were recorded in Bruker DPX250 (250 MHz for ^{1}H-NMR) and Bruker AV-III400 (400 MHz for ^{1}H-NMR; 100.6 MHz for ^{13}C-NMR) spectrometers using the appropriate deuterated solvent. Chemical shifts (δ) are given in ppm and the signals are referenced to the residual solvent peak.

High-resolution mass spectrometry analyses were measured in a MALDI-TOF UltrafleXtreme (Bruker Daltonics) spectrometer.

Transmission electron microscopy (TEM) images were recorded in a JEM 1400 transmission electron microscope operating at 120 kV. To visualize the organic shell of AuNP@PVP particles, a negative stain with uranium acetate was done.

UV-Vis absorption and extinction spectra were measured in a HP 8453 spectrophotometer in 1-cm quartz cells and using HPLC or spectroscopic quality solvents.

Fluorescence emission spectra were recorded in a PerkinElmer LS 55 spectrofluorometer. All samples were measured in 1-cm quartz fluorescence cells at 25 ± 0.1 ºC using HPLC or spectroscopic quality solvents.

Cyclic voltammograms were registered using a VSP 100 BIOLOGIC potentiostat. A three electrode conical electrochemical cell equipped with a glassy carbon electrode (WE, d = 1 mm), an auxiliary platinum electrode (CE, d = 1 mm), a saturated calomel electrode (SCE, RE) and an argon bubbling source was used. All the potentials are reported versus a SCE isolated from the working electrode by a salt bridge. All measurements were performed in anhydrous acetonitrile containing 0.1 M solution of *n*-Bu_4NPF_6, which acts as supporting electrolyte.

II. SYNTHESIS OF 1, (*Z*)-2, (*Z*)-3, (*Z*)-4 and (*Z*)-5

II.I Synthesis of 1

The heptathiolated derivative of β-cyclodextrin **1** was synthesized according to the procedure reported by Kaifer *et al*,[1] introducing an additional step based on a similar process described for γ-cyclodextrin[2] (Scheme S1). The synthetic procedure starts with the selective substitution of the primary hydroxyls of pristine β-CD by iodides to yield **5**, which is then peracetylated to enable proper purification by flash column chromatography of the iodated derivative **6**. Treatment of this compound with thiourea and subsequent hydrolysis in basic media of the isothiouronium groups formed and the acetate moieties furnished target ligand **1**.

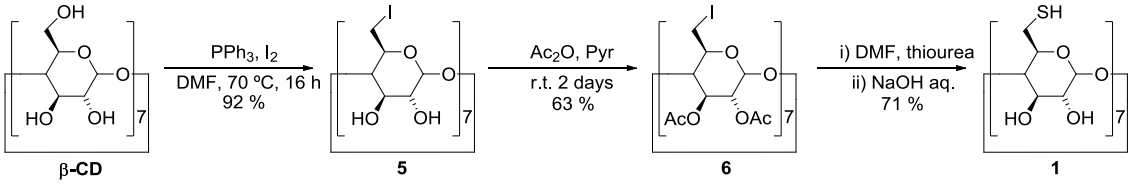

Scheme S1. Synthetic procedure for the preparation of **1**.

Per-6-iodo-β-cyclodextrin (5)

Triphenylphosphine (20.2 g, 77.0 mmol) was dissolved in dry DMF (80 mL) and iodine (20.2 g, 77.2 mmol) was carefully added during 10-15 minutes. Dry β-cyclodextrin (5 g, 4.4 mmol) was then added to the resulting dark-brown solution, which was stirred at 70 ºC under Ar atmosphere for 18 h. The resulting reaction mixture was concentrated under reduced pressure to half volume. The concentrated solution was adjusted to pH 9-10 by addition of 3 M sodium methoxide in methanol under cooling in an ice bath. Once at room temperature, the mixture was stirred for 30 minutes and was then poured over 400 mL of cold methanol under vigorous stirring to form a brownish precipitate. The precipitate was filtered, washed with methanol and air-dried. Soxhlet extraction with methanol of this solid was done until no more discoloration of the solvent could be seen, finally obtaining a clear brown solid (7.70 g, 92 % yield).**^{1}H-NMR (250 MHz, DMSO-d$_6$):** δ 6.05 (d, *J* = 6.5 Hz, 7H), 5.94 (d, *J* = 2.0 Hz, 7H), 4.99 (d, *J* = 2.0 Hz, 7H) 3.80 (d, *J* = 9.0 Hz, 7H), 3.54-3.68 (m, 14H), 3.24-3.47 (m, 21H). **^{13}C-NMR (100.6 MHz, DMSO-d$_6$):** δ 102.2, 86.0, 72.3, 72.0, 71.0, 9.5. **HRMS (MALDI-TOF):** m/z; calcd. for [$C_{42}H_{63}I_7O_{28}$+Na^+] 1926.671, found 1926.690.

Per-[(2,3-di-O-acetyl)-(6-iodo)]-β-cyclodextrin (6)

Per-6-iodo-β-cyclodextrin (5.0 g, 2.6 mmol) was dissolved in dry pyridine (15 mL, 186 mmol) and acetic anhydride (15 mL, 159 mmol) was added. The mixture was stirred under Ar atmosphere at room temperature for 2 days. Methanol (18 mL) was then added in 2 mL portions taking care that bubbling had finished before each new addition. The resulting mixture was poured over 500 mL 1.0 M HCl solution in water. The whole mixture was stirred for 5 min and then extracted with CH_2Cl_2 (4 x 75 mL), dried with Na_2SO_4, filtered and the solvent evaporated under reduced pressure to give a yellowish solid. Purification by flash column chromatography (Silica 60, 100 %

EtOAc) furnished **6** as a white solid (3.98 g, 63 % yield). **^{1}H-NMR (250 MHz, DMSO-d_6):** δ 5.34 (dd, J_1 = 8.1 Hz, J_2 = 9.9 Hz, 7H), 5.20 (d, J = 3.9 Hz, 7H), 4.84 (dd, J_1 = 3.9 Hz, J_2 = 9.9 Hz, 7H), 3.71-3.87 (m, 14H), 3.56-3.68 (m, 14H), 2.09 (s, 21H), 2.06 (s, 21H). **^{13}C-NMR (100.6 MHz, DMSO-d_6):** δ 170.7, 169.5, 96.7, 80.7, 70.5, 70.4, 70.2, 20.9, 8.0. **HRMS (MALDI-TOF):** m/z; calcd. for [$C_{70}H_{91}I_7O_{42}$+Na^+] 2514.820, found 2514.845.

Per-6-thio-β-cyclodextrin (1)

Per-[(2,3-di-*O*-acetyl)-(6-iodo)]-β-cyclodextrin (1.5 g, 0.6 mmol) was disolved in dry DMF (20 mL) and thiourea (0.35 g, 4.68 mmol) was added. The reaction mixture was stirred at 70 ºC under Ar atmosphere. After 19 h, DMF was removed under reduced pressure to give a yellow-orange oil. The oil obtained was dissolved in water (50 mL) and sodium hydroxide (2.43 g, 61 mmol) was added. The resulting mixture was stirred at reflux under nitrogen atmosphere for 1 h, which resulted in a color change from pale yellow to pale orange. Once at room temperature, the resulting suspension was acidified with 1.0 M $KHSO_4$ and the precipitate filtered off, washed thoroughly with distilled water and dried under vacuum to obtain compound **1** as a white solid (0.53 g, 71 % yield). **^{1}H-NMR (250 MHz, DMSO-d_6):** δ 5.94 (d, J = 6.5 Hz, 7H), 5.82 (s, 7H), 4.93 (d, J = 2.5 Hz, 7H), 3.50-3.87 (m, 14H), 3.05-3.50 (m, 21H), 2.75 (m, 7H), 2.13 (t, J = 8 Hz, 7H). **^{13}C-NMR (100.6 MHz, DMSO-d_6):** δ 102.2, 84.9, 72.6, 72.3, 72.0, 26.0. **HRMS (MALDI-TOF):** m/z; calcd. for [$C_{42}H_{70}O_{28}S_7$+Na^+] 1269.199, found 1269.217.

II.II Synthesis of (*Z*)-2, (*Z*)-3, (*Z*)-4 and (*Z*)-5

General procedure for the synthesis of (*Z*)-2, (*Z*)-3, (*Z*)-4 and (*Z*)-5

Commercially available (*E*)-**2**, (*E*)-**3**, (*E*)-**4** and (*E*)-**5** (80 mg) were dissolved in acetonitrile (10 mL). The resulting solutions were degassed with Ar and irradiated at 365 nm with a 4 W UV lamp during 24 h (Scheme S2) to achieve the photostationary state. The solvent was evaporated under reduced pressure and the solid obtained was purified.

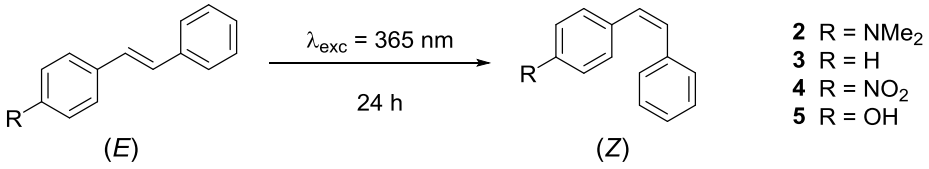

Scheme S2. Preparation of the *Z* isomer of the stilbenes of interest.

(*Z*)-2

(*Z*)-**2** was purified from the reaction mixture by successive fractional precipitation of the (*E*)-**2** isomer. After evaporation of the solvent the residue was resuspended in 10 mL of *n*-hexane and digested at -32 ºC for 24 h. The suspension obtained was filtered through a tight cotton plug and the solvent evaporated under reduced pressure. The residue was again resuspended in 5 mL of *n*-hexane and digested at -32 ºC for 24 h. The precipitate was filtered, the solvent evaporated and the resuspension-precipitation

operation was repeated one more time with 2 mL of *n*-hexane. After evaporation of the final filtrate, an amber oil was obtained (35 mg, 44 % yield) with a 98:2 (*Z*)-**2**:(*E*)-**2** ratio. Further purification of this mixture could not be achieved by flash column chromatography. **^{1}H-NMR (400 MHz, DMSO-d$_6$):** δ 7.30-7.24 (m, 4H), 7.20 (m, 1H), 7.06 (m, 2H), 6.57 (m, 2H), 6.46 (d, *J* = 12.0 Hz, 1H), 6.38 (d, *J* = 12.0 Hz, 1H), 2.87 (s, 6H). **^{13}C-NMR (100 MHz, DMSO-d$_6$):** δ 149.48, 137.83, 130.22, 129.51, 128.31, 128.30, 126.74, 126.17, 124.05, 111.67, 39.85.

(*Z*)-3

(*Z*)-**3** was purified from the reaction mixture by flash column chromatography (Silica 60, *n*-hexane:$CHCl_3$ 10:1), obtaining a colorless oil (20 mg, 25 % yield). **^{1}H-NMR (400 MHz, DMSO-d$_6$):** δ 7.31-7.19 (m, 10H), 6.65 (s, 2H). **^{13}C-NMR (100 MHz, DMSO-d$_6$):** δ 136.82, 130.08, 128.48, 128.34, 127.28.

(*Z*)-4

(*Z*)-**4** was purified from the reaction mixture by successive fractional precipitation of the (*E*)-**4** isomer. After evaporation of the solvent the residue was resuspended in 10 mL of *n*-hexane and digested at -32 ºC for 24 h. The suspension obtained was filtered through a tight cotton plug and the solvent evaporated under reduced pressure. The residue was again resuspended in 5 mL of *n*-hexane and digested at -32 ºC for 24 h. The precipitate was filtered, the solvent evaporated and the resuspension-precipitation operation was repeated one more time with 2 mL of *n*-hexane. After evaporation of the final filtrate, a yellow oil was obtained (18 mg, 22 % yield) with a 97:3 (*Z*)-**4**:(*E*)-**4** ratio. Further purification of this mixture could not be achieved by flash column chromatography. **^{1}H-NMR (400 MHz, DMSO-d$_6$):** δ 8.13 (d, *J* = 8.9 Hz, 2H), 7.47 (d, *J* = 8.9 Hz, 2H), 7.34-7.27 (m, 3H), 7.22 (m, 2H), 6.88 (d, *J* = 12.35 Hz, 1H), 6.76 (d, *J* = 12.35 Hz, 1H). **^{13}C-NMR (100 MHz, DMSO-d$_6$):** δ 146.52, 136.31, 133.90, 130.11, 129.01, 128.98, 128.54, 128.35, 124.02, 118.42.

(*Z*)-5

(*Z*)-**5** was purified from the reaction mixture by successive fractional precipitation of the (*E*)-**5** isomer. After evaporation of the solvent the residue was resuspended in 10 mL of *n*-hexane and digested at -32 ºC for 24 h. The suspension obtained was filtered through a tight cotton plug and the solvent evaporated under reduced pressure. The residue was again resuspended in 5 mL of *n*-hexane and digested at -32 ºC for 24 h. The precipitate was filtered, the solvent evaporated and the resuspension-precipitation operation was repeated one more time with 2 mL of *n*-hexane. After evaporation of the final filtrate, a yellow oil was obtained (13 mg, 16 % yield) with a 98:2 (*Z*)-**5**:(*E*)-**5** ratio. Further purification of this mixture could not be achieved by flash column chromatography. **^{1}H-NMR (400 MHz, DMSO-d$_6$):** δ 9.50 (s, 1H), 7.30-7.16 (m, 5H), 7.04 (d, *J* = 8.4 Hz, 2H), 6.62 (d, *J* = 8.4 Hz, 2H), 6.50 (d, *J* = 12.35 Hz, 1H), 6.45 (d, *J* = 12.35 Hz, 1H). **^{13}C-NMR (100 MHz, DMSO-d$_6$):** δ 157.09, 137.74, 130.41, 130.25, 128.78, 128.70, 127.93, 127.72, 127.34, 115.48.

III. PREPARATION OF GOLD NANOPARTICLES

III.I Synthesis of AuNP@1 and AuNP@PVP

AuNP@**1** and AuNP@PVP were synthesized through a two-step process (Scheme S3). First, ~15 nm-in-diameter AuNP@citrate were synthesized according to the Turkevich-Frens method introducing the modifications needed to achieve the desired particle size.[3,4,5] The next step involved the ligand exchange process of citrate ions by the desired stabilizer.[6,7]

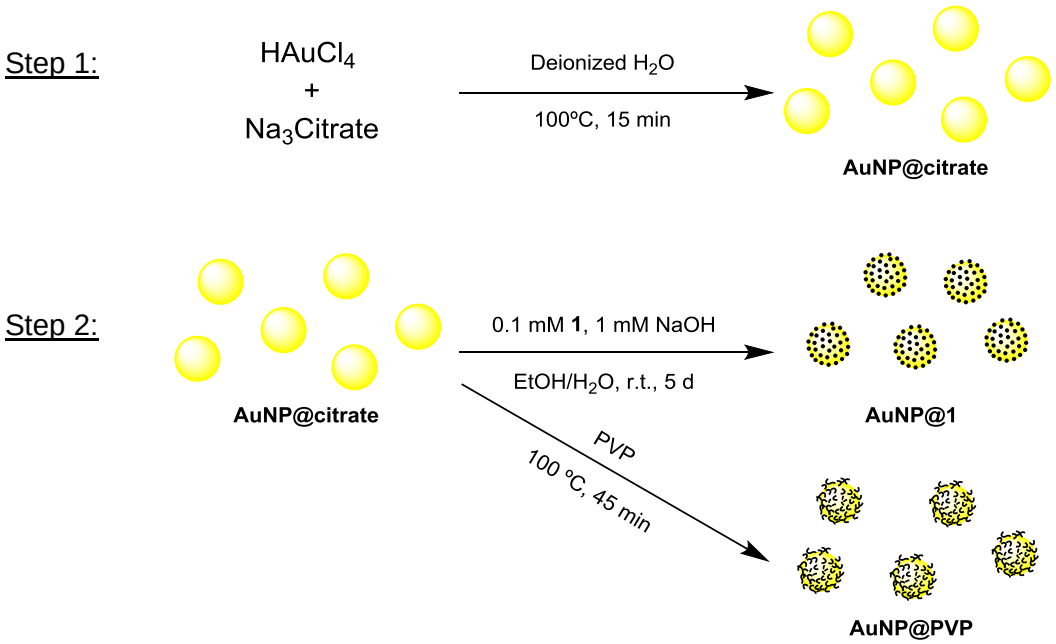

Scheme S3. Two-step process used for the preparation of AuNP@**1** and AuNP@PVP.

AuNP@citrate

A solution of chloroauric acid (0.15 mM) in deionized water (200 mL) was heated to boiling under stirring. To this solution, a pre-heated solution (90 ºC) of trisodium citrate (30 mM) in deionized water (20 mL) was rapidly added maintaining a gentle boiling. Rapidly, the color changed from light yellow to deep-wine red. Boiling was maintained for 10-15 minutes and the reaction mixture was allowed to cool down to room temperature. Finally, the colloidal suspension of AuNP@citrate was stored at 4 ºC in the fridge. AuNP@citrate were characterized by means of UV-Vis spectroscopy and TEM, and their concentration was determined to be 8.27 nM (ε_{max} = 4.152·10^{8} M^{-1}·cm^{-1}) as discussed below (see Section III.III).

AuNP@1

To an aqueous colloidal suspension of freshly prepared AuNP@citrate (*c* = 8.27 nM), a mixture of **1** and NaOH in ethanol was added so that their final concentrations were 0.1 mM and 1 mM, respectively (e.g. 20 mL of a 1.0 mM ligand and 10 mM NaOH solution per 180 mL AuNP@citrate suspension). The resulting mixture was left to stir at room

temperature for 5 days. Afterwards, the mixture was diluted to one half with acetonitrile and the resulting AuNP@**1** suspension was centrifuged at 11500 rpm during 15 minutes. The pelleted AuNPs were resuspended in DMF (15 mL) and dialyzed against this solvent during 3 days changing the solvent every 24 h. Acetonitrile was then added (150 mL) and the colloidal suspension was centrifuged at 12000 rpm during 20 minutes. The pelleted AuNPs were resuspended in deionized water (10 mL) upon sonication. AuNP@**1** were characterized by means of UV-Vis spectroscopy, ^{1}H NMR and TEM. From the average particle diameter (14 nm) and the outer diameter of β-CD (1.54 nm [8]), the number of **1** molecules attached to AuNP@**1** was estimated to be ~ 331 molecules/nanoparticle assuming full surface coverage.

AuNP@PVP

To a boiling aqueous colloidal suspension of freshly prepared AuNP@citrate (50 mL, *c* = 8.27·nM), 2.5 mL of a 0.2 mg/mL polyvinylpyrrolidone solution were added. The reaction mixture was allowed to boil for additional 35-45 minutes. The final colloidal suspension was allowed to cool down to room temperature, concentrated by centrifugation at 4000 rpm during 1 h and stored at 4ºC in the fridge. AuNP@PVP were characterized by means of UV-Vis spectroscopy and TEM.

III.II Synthesis of AuNP-s@1

The preparation of the smaller AuNP@**1** (AuNP-s@**1**) was done in a single step according to the reported procedure described by Kaifer *et al* (Scheme S4).[9]

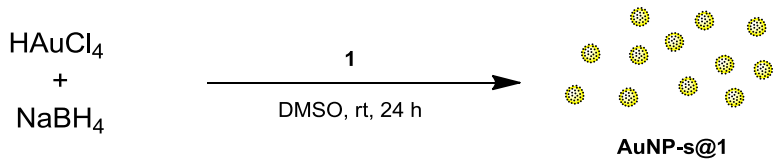

Scheme S4. Preparation of the ~5-nm-in-diameter AuNP-s@**1**.

A solution of chloroauric acid (50 mg) in DMSO (20 mL) was quickly mixed with another solution containing $NaBH_4$ (75.5 mg) and **1** (12.2 mg). The reaction mixture changed in color and turned deep brown immediately but the reaction was allowed to stir for 24 h. Then acetonitrile was added (40 mL) and the precipitated gold colloid was centrifuged at 10000 rpm during 5 minutes. The pelleted AuNPs were redissolved in DMSO (20 mL), precipitated again by the addition of acetonitrile (20 mL) and centrifuged at 10000 rpm for 10 minutes. Finally, the pelleted AuNPs were resuspended in ethanol (60 mL), isolated by centrifugation at 10000 rpm during 10 minutes and dried under vacuum at room temperature. AuNP-s@**1** were characterized by means of UV-Vis spectroscopy and TEM.

III.III Determination of AuNP concentration in aqueous suspension

From the extinction spectrum of AuNPs and the extinction coefficient of the maximum of the surface plasmon resonance band, the concentration of AuNPs in aqueous suspension was determined using the following double logarithm equation:[10]

$$\ln \varepsilon = k \ln D + a \quad (1)$$

In this expression, ε is the extinction coefficient (given in M^{-1} cm^{-1}), D is the core diameter of the nanoparticles (given in nm and determined from TEM measurements), and k = 3.32111 and a = 10.80505 are pre-established parameters determined for citrate-stabilized spherical AuNPs in water. As an approximation,[10] we also took these parameter values for the rest of nanoparticles investigated in this work when suspended in aqueous media (AuNP@**1**, AuNP@PVP and AuNP-s@**1**).

IV. CHARACTERIZATION OF GOLD NANOPARTICLES

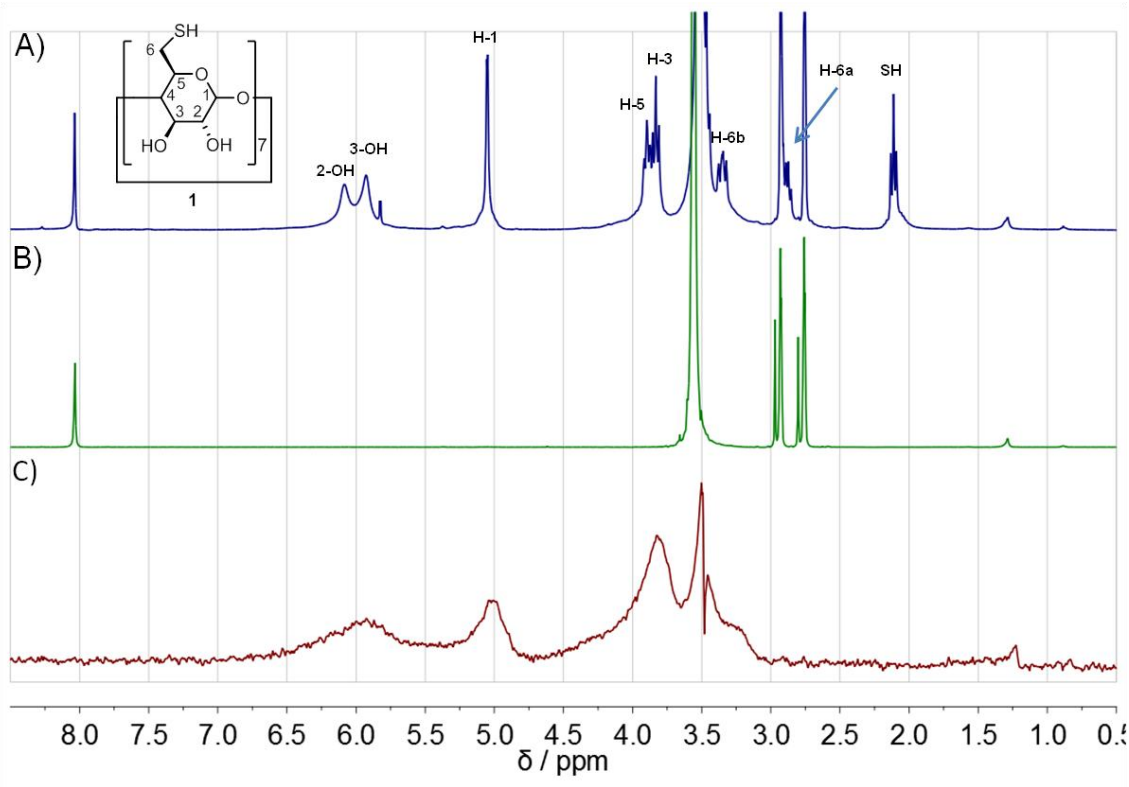

Fig. S1. A) ^{1}H-NMR (400 MHz, DMF-d_7) spectrum of free ligand **1**. B) ^{1}H-NMR (400 MHz, DMF-d_7) spectrum of AuNP@**1**, where no signals were observed for free ligand **1**. C) 1D DOSY ^{1}H-NMR (400 MHz, DMF-d_7) spectrum of the same sample, which was programmed to selectively detect the signals of ligands that are directly attached to the surface of the gold nanoparticles (i.e. those presenting the lower diffusion coefficients). Different features of this spectrum supports assignment to AuNP-tethered **1** molecules: (i) loss of the –S*H* signal at δ = 2.1 ppm due to S-Au bond formation; (ii) broadening of the 2-O*H*, 3-O*H* and *H*-1, *H*-3 and *H*-5 signals and disappearance of *H*-6a signal at δ = 2.79 ppm owing to the metal effect on the spin relaxation rate of nearby nuclei.

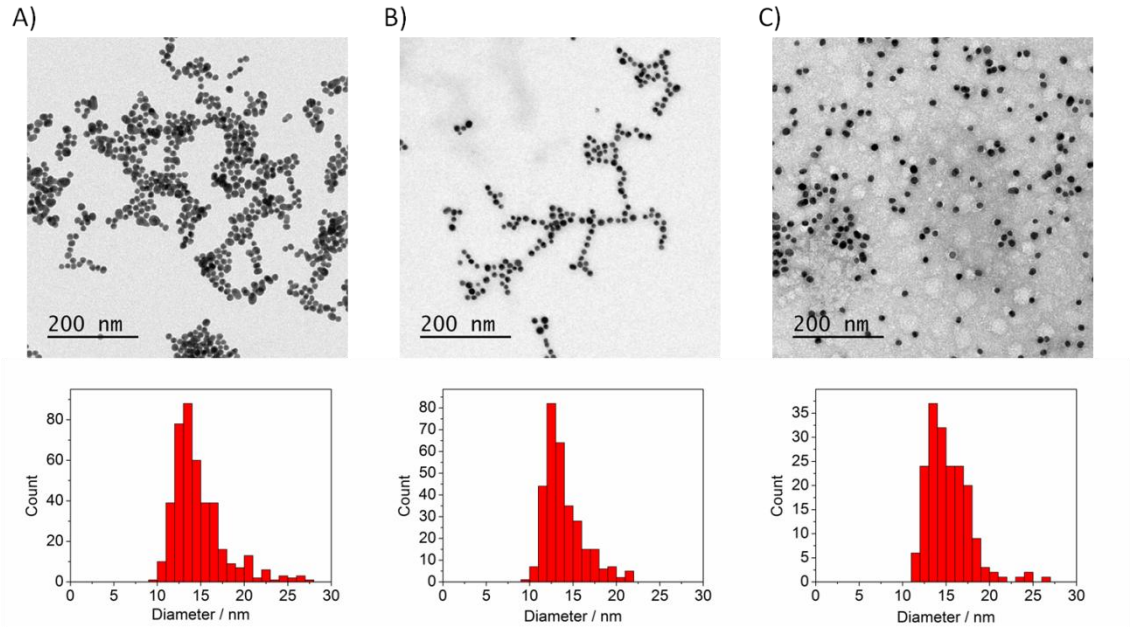

Fig. S2. TEM images and size histograms of AuNP@citrate (A, diameter = 15 ± 3 nm), AuNP@**1** (B, diameter = 14 ± 2 nm) and AuNP@PVP (C, diameter = 15 ± 2 nm).

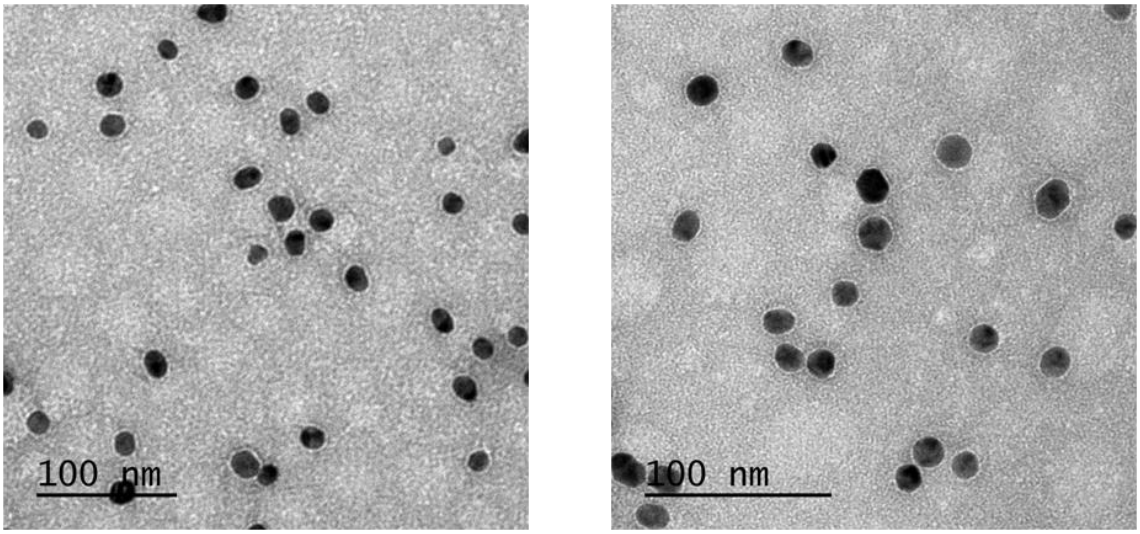

Fig. S3. Amplified TEM images of several AuNP@PVP, where sample negative staining with uranium acetate allows visualization of the organic shell. An average PVP shell thickness of 1.4 nm could be determined in this way.

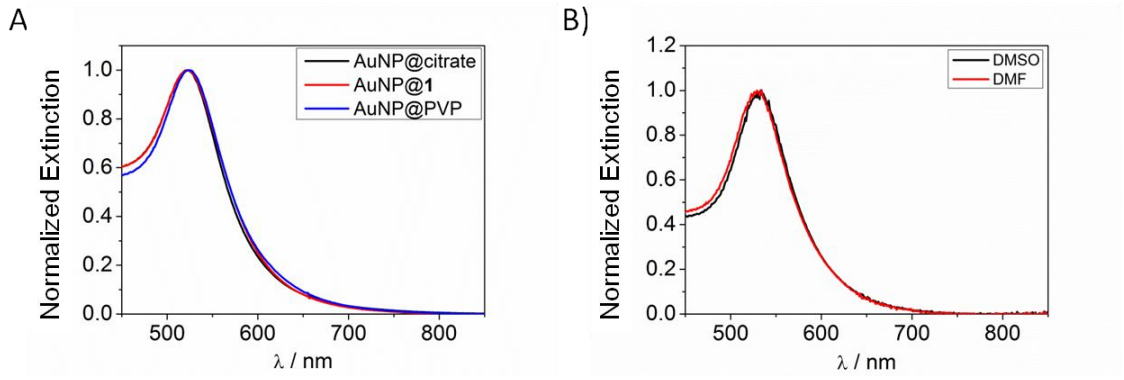

Fig. S4. A) Extinction spectra of AuNPs coated with different stabilizers in aqueous suspension. Negligible differences are observed which, in combination with the histograms shown in Figure S1, demonstrates that AuNPs remain essentially unaltered upon ligand exchange. B) Extinction spectra of AuNP@**1** in DMSO and DMF, which confirm the stability enhancement of AuNPs in organic solvents upon replacement of citrate ligands with **1**.

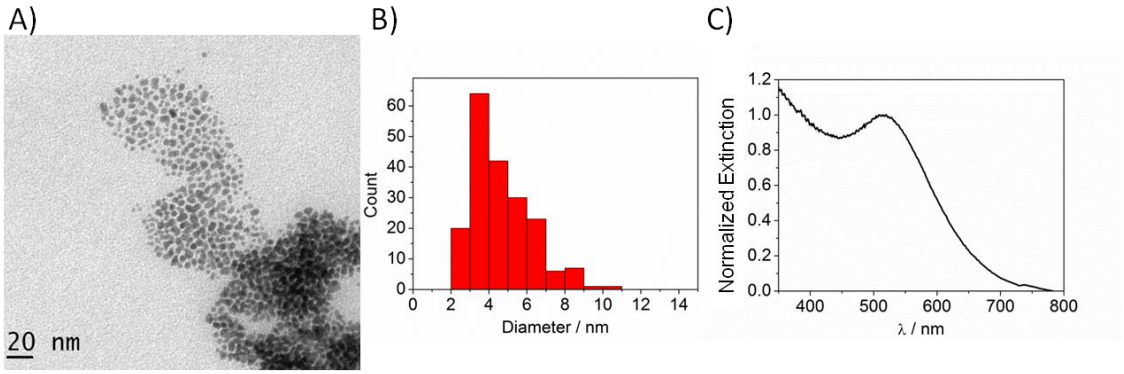

Fig. S5. A) TEM image of AuNP-s@**1**. B) Size distribution of AuNP-s@**1**, which have a mean diameter of 5 ± 2 nm. C) Extinction spectrum of an aqueous suspension of AuNP-s@**1** (ε_{max} = 1.033·10^{7} M^{-1}·cm^{-1}).

V. SUPRAMOLECULAR HOST-GUEST CHARACTERIZATION

The association constant of the 1:1 CD-stilbene complexes can be defined as the equilibrium constant of the following reaction:

$$\text{CD} + \text{stilbene} \rightleftharpoons \text{CD:stilbene}$$

$$K_a = \frac{[\text{CD:stilbene}]}{[\text{CD}][\text{stilbene}]} \quad (2)$$

The value of K_a can be obtained from the observed fluorescence enhancement (or quenching) (F/F_0) as a function of the concentration of CD added ($[CD]_0$ = 0, 0.1, 0.5, 1, 2, 3, 5, 7 and 10 mM) to a solution of constant concentration of stilbene ($2 \cdot 10^{-5}$ M):[11]

$$\frac{F}{F_0} = 1 + \left(\frac{F_\infty}{F_0} - 1\right) \frac{[\text{CD}]_0 K_a}{1 + [\text{CD}]_0 K_a} \quad (3)$$

In this expression F is the fluorescence intensity in the presence of CD for a certain CD:stilbene mixture, F_0 is the fluorescence intensity in the absence of CD, and F_∞ is the fluorescence intensity when all guest molecules are complexed (i.e. at infinite concentration of CD).

The calculated K_a values for the six different stilbenes studied are summarized in Table S1, where nonthiolated β-CD was selected as a supramolecular host owing to its larger solubility in water with respect to ligand **1**. Because of the low solubility in water of the (*E*)-isomer of stilbene derivatives **2**-**4**, their K_a values could not be determined in the same medium where our photocatalytic experiments were conducted (water:acetonitrile 94:6). Instead, a solvent mixture with a larger content of acetonitrile had to be used (water:acetonitrile 75:25). For this reason, β-CD:(*Z*)-stilbene K_a values were measured in both media, which demonstrated that host-guest association constants decreased in *ca.* 85% for (*Z*)-**2**, 70% for (*Z*)-**3** and 76% for (*Z*)-**4** when increasing acetonitrile concentration. This allows rough estimates of β-CD:(*E*)-stilbene K_a values in water:acetonitrile 94:6 to be made for **2**-**4**: *ca*. 8000 M^{-1} for (*E*)-**2**, 600 M^{-1} for (*E*)-**3** and 200 M^{-1} for (*E*)-**4**. In the case of stilbene **5**, its both isomers where soluble enough in aqueous media as to allow direct measurement of their association constant with β-CD in water:acetonitrile 94:6.

Table S1. Association constants determined for the supramolecular complexes formed between β-CD and the *Z*- and *E*-isomers of the stilbenes of interest.

Compound	K_a (*Z*-isomer) / M^{-1}		K_a (*E*-isomer) / M^{-1}
	Water:acetonitrile 94:6	Water:acetonitrile 75:25	Water:acetonitrile 75:25
2	1783 ± 265	291 ± 64	1306 ± 321
3	140 ± 13	44 ± 14	190 ± 58
4	106 ± 19	25 ± 6	48 ± 14
5	724 ± 223	-	1056 ±163[a)]

[a)] In water:acetonitrile 94:6.

VI. PHOTOCHEMICAL AND THERMAL STILBENE ISOMERIZATION

Control experiments of the pure photochemical and thermal *Z* → *E* and *E* → *Z* isomerization of **2**-**4** were carried out in the same medium as our photocatalytic experiments (water:acetonitrile 94:6).

Photochemical isomerization: 2 10^{-6} M solutions of the *Z*- and *E*-isomers of **2**-**4** in water:acetonitrile 94:6 were purged with Ar and irradiated with a UV-lamp (4 W) until obtaining the corresponding photostationary states (PSS). Owing to the different UV-vis absorption spectra of these compounds (Figure S6), *Z* → *E* photoisomerization was induced by irradiation at 254 nm, while *E* → *Z* photoisomerization was investigated by irradiation at 365 nm. After illumination, the photoisomerization conversions were determined by comparison of the UV-vis absorption spectra of the PSS mixtures with those of the pure *Z*- and *E*-isomers (Table S2).

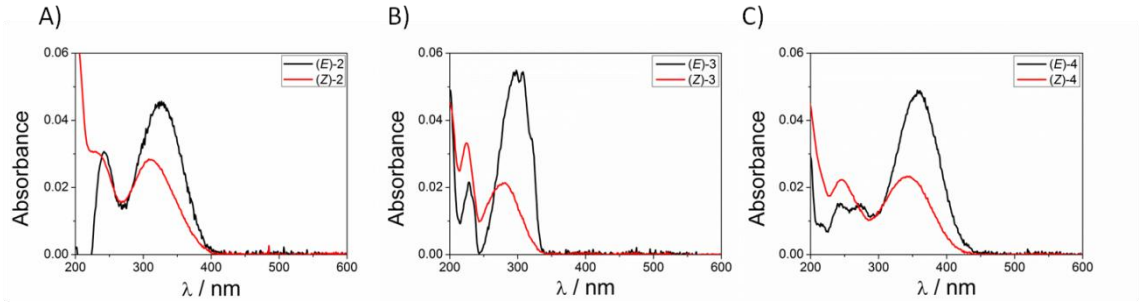

Fig. S6. Absorbance spectra in water:acetonitrile 94:6 of: A) (*E*)-**2** and (*Z*)-**2** (c = 2·10^{-6} M); B) (*E*)-**3** and (*Z*)-**3** (c = 2·10^{-6} M); C) (*E*)-**4** and (*Z*)-**4** (c = 2·10^{-6} M).

Table S2. Photoisomerization conversions (%) of **2**-**4** upon direct UV irradiation in water:acetonitrile 94:6.

Compound	*Z* → *E*	*E* → *Z*
2	41	83
3	48	92
4	64	68

Thermal isomerization: Samples containing *ca.* 1 mg of the corresponding *Z*- or *E*-stilbene suspended in 500 μL of D_2O:CD_3CN 94:6 were purged with Ar and heated in an oil bath under reflux (~373 K) for 2 h (i.e. the same duration as in our photocatalytic experiments). Afterwards the samples were cooled in an ice bath, 500 μL of DMSO-d_6 were added to completely dissolve the solid and they were analyzed by ^{1}H-NMR. The conversion of the *Z* isomer to the *E* form was determined from the integration of the signals for the protons at the *ortho* position of the substituted phenyl ring. To unravel supramolecular and/or catalytic effects on the bulk thermal isomerization of **2**-**4**, additional controls were conducted upon addition of β-CD and AuNP@**1** to the sample at the same concentrations as in the photocatalytic experiments. Moreover, pure

thermal isomerization of the stilbene derivatives was also attempted in DMSO-d_6, which allowed reaching higher heating temperatures (373 K and 423 K). All the results obtained in these experiments are shown in Table S3.

Table S3. Thermal isomerization conversions (%) of **2**-**4** upon bulk heating.[a)]

T (K)	Solvent	β-CD	AuNP@1	$Z \rightarrow E$			$E \rightarrow Z$		
				2	**3**	**4**	**2**	**3**	**4**
373	D_2O:CD_3CN	No	No	10	0	0	0	0	0
373	D_2O:CD_3CN	Yes	No	12	0	0	0	0	0
373	D_2O:CD_3CN	No	Yes	26	0	29	0	0	0
373	DMSO-d_6	No	Yes	2	0	2	0	0	0
423	DMSO-d_6	No	No	99	2	3	0	0	0

[a)] Experiments conducted in deuterated water:acetonitrile 94:6 under reflux (~373 K) for 2 h and in DMSO-d_6 for 30 min (423 K). $c_{\beta\text{-CD}}$ = 15 μM. $c_{\text{AuNP@1}}$ = 45 nM.

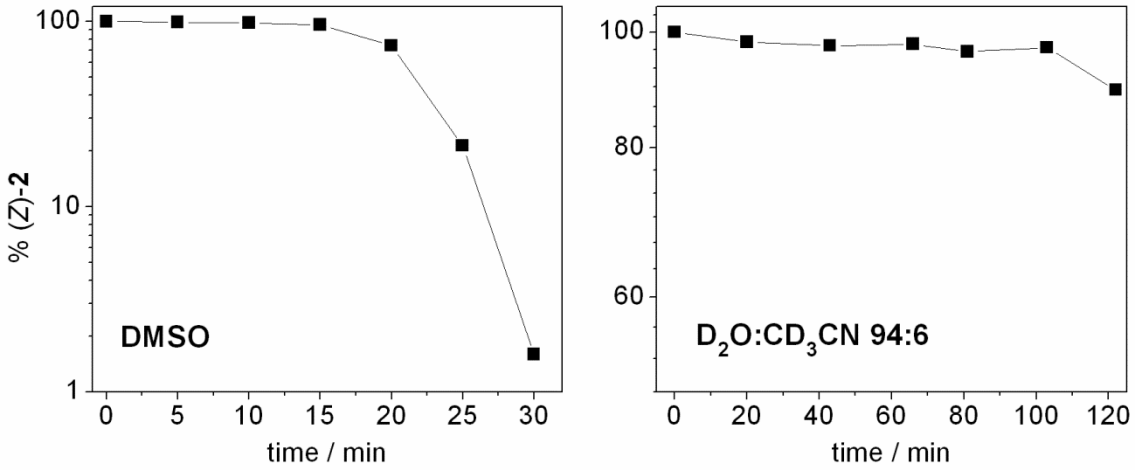

Fig. S7. $Z \rightarrow E$ isomerization kinetics of (*Z*)-**2** in the absence of AuNPs and upon bulk heating at 423 K in DMSO-d_6 and ~373 K in D_2O:CD_3CN 94:6. Clearly, none of them follows a logarithmic first-order reaction rate, as expected for this simple unimolecular reaction. Instead, an induction period with negligible conversion is first observed in both cases (*t* = 0-15 min and 0-100 min, respectively), which is then followed by a sudden rise of the reaction rate (t > 15 min and 100 min, respectively). Although the actual mechanism accounting for this behavior is not currently clear to us, it unambiguously indicates that, at these conditions, the reaction proceeds through a multistep process requiring the formation of a thermally activated species. This means that the simple unimolecular mechanism of $Z \rightarrow E$ isomerization of (*Z*)-**2** does not take place at such temperatures, as also observed for (*Z*)-**3** and (*Z*)-**4** and predicted from our theoretical calculations (see below).

VII. PHOTOCATALYTIC STUDIES

Photocatalysis experiments were carried out using the second harmonic of a Nd:YAG pulsed laser as excitation source (λ_{exc} = 532 nm) operating at a frequency of 10 Hz and with a round spot size of 0.8 mm in diameter.

Sample preparation and reaction: 500 μL of an aqueous AuNP suspension (prepared from concentrated stock suspensions) were put in a GC vial equipped with a septum stopper. The suspension was purged with Ar and irradiated at 100 mW (10 mJ/pulse) during 30 minutes prior to the addition of the reactant molecules. During this time, AuNPs assemblies formed during the purification process (in the case of AuNP@**1**) and attributed to H-bonding between cyclodextrin molecules were disaggregated. Afterwards, the stilbene derivative of interest was added (30 μL from a 200 mM stock solution in acetonitrile). The resulting mixture was irradiated under stirring at 532 nm during 30, 60 or 120 minutes. All blank samples for control experiments were pre-treated in the same way (100 mW, 30 min) before the addition of the reactant molecules. When required, other compounds were added to the reaction mixtures before irradiation (e.g. β-CD).

Sample work-up: After irradiation, the reaction mixture was diluted with acetonitrile (6 mL) and centrifuged at 12000 rpm during 15 minutes. The supernatant was isolated and evaporated under reduced pressure. The final residue was dissolved in deuterated DMSO for further ^{1}H-NMR analysis. Determination of the final $Z \rightarrow E$ (or $E \rightarrow Z$) isomerization conversion for the photocatalytic studies was determined by integration of the signals for the protons at the *ortho* position of the substituted phenyl ring (Figure S8). Most photocatalytic results obtained in this way are shown in Table 1 in the main text, although the yields determined in some other additional experiments are given in Table S4.

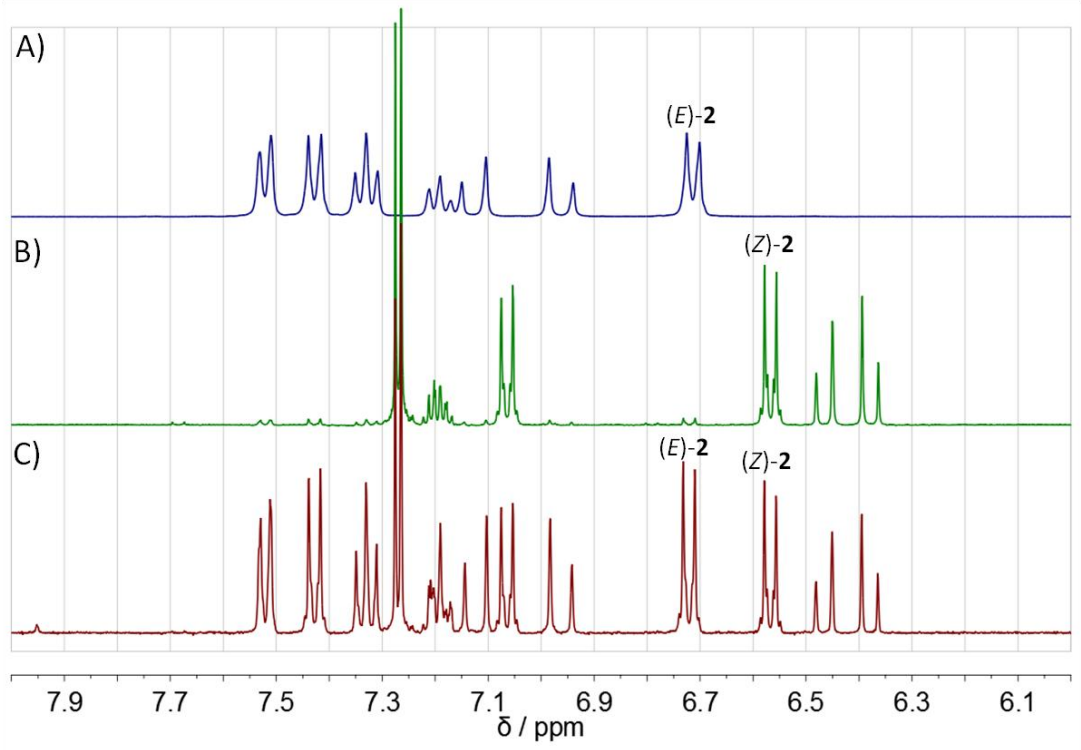

Fig. S8. ^{1}H-NMR spectra (400 MHz, DMSO-d_6) of A) (*E*)-**2** and B) (*Z*)-**2**. C) ^{1}H-NMR spectrum (400 MHz, DMSO-d_6) of the reaction mixture obtained after irradiation of (*Z*)-**2** at λ = 532 nm in the presence of AuNP@**1**. Clearly, selective $Z \rightarrow E$ isomerization takes places under visible light irradiation due to the photocatalytic activity of gold nanoparticles. The $Z \rightarrow E$ conversion obtained for this experiment was 55% as calculated from the integrals corresponding to the proton signals indicated in the spectrum.

Table S4. $Z \rightarrow E$ (or $E \rightarrow Z$) photocatalytic isomerization conversions.[a)]

Entry	Substrate	Catalyst	Irraditation power (mW)	Irraditation time (h)	Yield (%)
1	(*E*)-**2**	AuNP@**1**	300	2	0
2	(*Z*)-**3**	AuNP@**1**	300	2	8
3	(*Z*)-**3**	AuNP@citrate	300	2	3
4	(*Z*)-**4**	AuNP@**1**	300	2	15
5	(*Z*)-**4**	AuNP@citrate	300	2	6
6	(*Z*)-**5**	AuNP@**1**	300	2	88
7	(*Z*)-**5**	AuNP@**1**	-	2	17
8	(*Z*)-**5**	-	-	2	0

[a)] $c_{catalyst}$ = 45 nM; $c_{substrate}$ = 11.3 mM; room temperature.

Recycling experiments: At the end of a photocatalytic experiment, the reaction mixture was diluted with acetonitrile (1 mL) and centrifuged in an *eppendorf* tube at 11000 rpm during 8 min. The supernatant was isolated for further ^{1}H-NMR analysis of the reaction conversion and the pelleted AuNP@**1** were resuspended in deionized water (500 μL) under sonication for the next photocatalytic cycle. The efficiency of this process of catalyst recovery was ~70 %. A small amount of the recovered nanoparticles were examined by TEM to evaluate the occurrence of catalyst photodegradation. As observed in Figure S9A-B, the formation of very small gold nanostructures of ~2-7 nm in size was found, which we ascribed to light-induced ablation of some of the initial ~15-nm-in-diameter AuNP@**1**. Importantly, such process did not take place during the pre-treatment of the nanoparticles at low irradiation power (100 mW, 30 min), but during the photocatalytic experiments involving higher light intensities and longer illumination times (300 mW, 2 h). By statistically analyzing the sizes of these two populations of NPs for several TEM images and assuming equal density, we could conclude that between 1 - 6 % of the initial mass of AuNP@**1** was photodegraded.

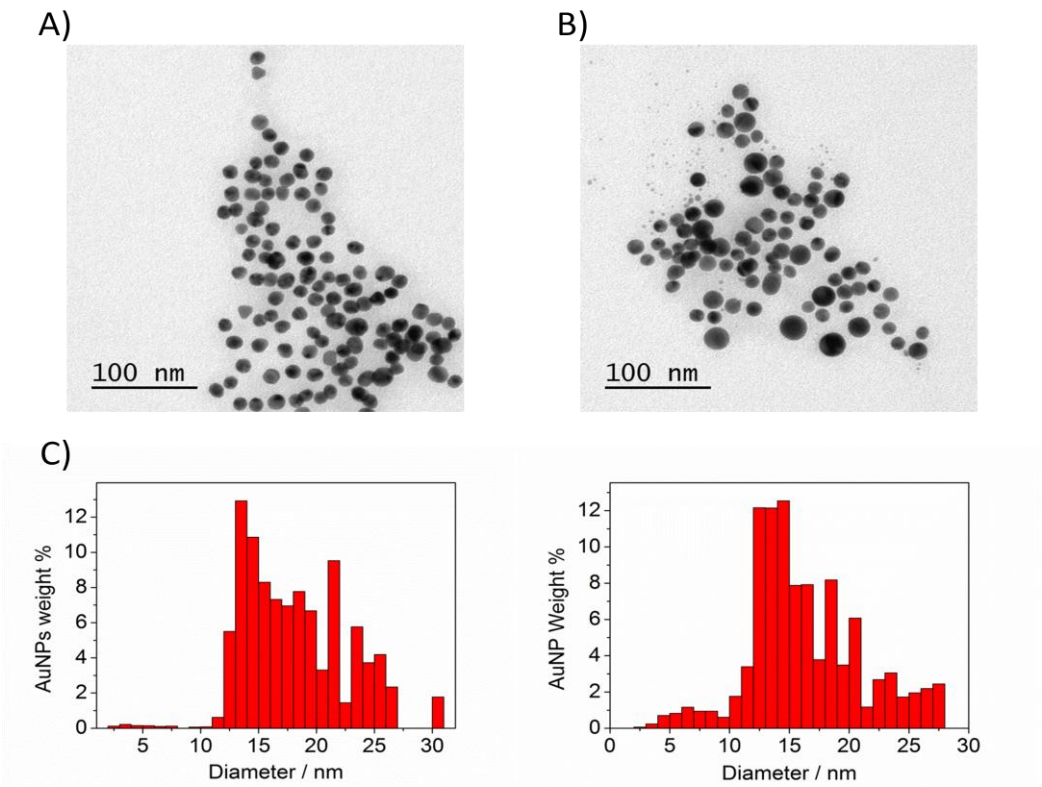

Fig. S9. A-B) Representative TEM images of A) pre-treated AuNP@**1** (100 mW, 30 min) and B) recovered AuNP@**1** after one photocatalytic experiment (300 mW, 2 h). C) Weight (%) distribution of the irradiated AuNP@**1** after two independent assays (300 mW, 2 h). The population of the small AuNPs formed upon photodegradation of the initial AuNP@**1** accounted for a 1-6 % of the total catalyst.

Control experiments with AuNP-s@**1**: To rule out increased photocatalytic activity due to the formation of very small AuNPs upon photodegradation of AuNP@**1**, we conducted several photocatalytic experiments of the $Z \rightarrow E$ isomerization of **2** with AuNP-s@**1** of ~5-nm-in-diameter. As shown in Table S5, the optimal irradiation conditions established for AuNP@**1** were applied, while AuNP-s@**1** concentration was selected to: (a) match the extinction at the irradiation wavelength of the AuNP@**1** suspensions used in the best catalytic experiments (c ~ 1.94·μM, entry 1); (b) match the total catalyst surface area of the AuNP@**1** suspensions used in the best catalytic experiments (c ~ 420 nM, entry 2).

Table S5. $Z \rightarrow E$ isomerization conversions of the control experiments with AuNP-s@**1**.

Entry	$c_{catalyst}$ (nM)	Irradiation power (mW)	Irradiation time (h)	Yield (%)
1	1940	300	2	18
2	420	300	2	8

VIII. THEORETICAL CALCULATIONS

The calculations presented in this work are aimed at evaluating the rotational barriers around the double bond of substitued stilbenes **2**-**5** in their neutral and oxidized (**2**$^{\bullet+}$-**5**$^{\bullet+}$**)** form. Calculations have been performed with the Gaussian09 package[12] and using the MPWB1K functional in combination with the 6-311+G(2d,p)[13,14] basis set. We have chosen the MPWB1K functional, with a high percentage of exact exchange (44%), because previous studies for radical cations have shown that GGA or hybrid DFT methods with small percentage of exact exchange tend to overstabilize structures with a too delocalized electron hole, MPWB1K providing good results compared to high level post-Hartree Fock methods.[15,16] For neutral species, and due to the multireference character of the transition structure, energy barriers have been computed from unrestricted broken symmetry calculations. Nevertheless, in order to assess the quality of this level of theory, values of the rotational barrier for **3** and **3**$^{\bullet+}$ (unsubstituted stilbene) were compared with single point CASPT2 calculations, at the optimized MPWB1K/6-311++G(2d,p) geometries, using a (6,6) active space. This active space includes π orbitals involving the double bond of interest for the rotation and the adjacent rings. CASPT2 calculations were carried out with the Molcas8 package[17] and all atoms were represented with the ANO-S basis sets, which shows a [2s1p] contraction for H and a [3s2p1d] contraction for C, N, O.[18] Table S6 shows that, for both **3** and **3**$^{\bullet+}$, MPWB1K reproduces well the values obtained with the more accurate CASPT2 method.[19,20] Interestingly, the energy barrier for the rotation around the double bond is significantly lower in **3**$^{\bullet+}$ than in **3**.

Table S6. Potential energy barrier ($\Delta \mathbf{U}_{iso}$, in kJ mol^{-1}) for the rotation around the double bond of stilbene computed at the MPWB1K/6-311+G(2d,p)[a] and CASPT2(6,6)/ANO-S levels of theory.

	3	**3**$^{\bullet+}$
CASPT2	188.4	129.8
MPWB1K	178.9	110.1

[a] The energy of the TS has been obtained from broken symmetry calculations.

The effect of substitution on the relative stabilities of isomers *Z* and *E* and on the height of the rotational barrier for their interconversion has been evaluated for compounds **2**-**5** and **2**$^{\bullet+}$-**5**$^{\bullet+}$. Results are reported in Table S7, along with the corresponding calculated ionization potentials (eV) of the (*Z*)-isomers. These values indicate that the energy barrier is not significantly affected by substitution (**2**, **3**, **4** and **5**), and that in all cases oxidation lowers this barrier and stabilizes isomer *E* over *Z*. At this point, *Z*→*E* isomerization is both thermodynamically and kinetically much more likely to occur in the oxidized rather than in the neutral form. For this reason, the efficiency of the process is expected to depend on the ionization potential, which determines how easily the neutral molecule can be oxidized. Our calculations indicate that **2** and **5** present by far the lowest ionization potentials among the molecules that have been considered, and are therefore the most prone to oxidation and consequently isomerization.

Table S7. Relative stabilities of isomers *Z* and *E* ($\Delta G_{Z\text{-}E}$, in kJ mol^{-1}), $Z \rightarrow E$ isomerization energy barriers (ΔG_{iso}, in kJ mol^{-1}) of **2**-**5** and **2**$^{\bullet+}$-**5**$^{\bullet+}$ computed at the MPWB1K/6-311+G(2d,p) level of theory. Calculated ionization energies (**IE**, in eV) are also given for (*Z*)-**2**, (*Z*)-**3**, (*Z*)-**4** and (*Z*)-**5**.

Reactant	$\Delta G_{Z\text{-}E}$	ΔG_{iso}	IE	Reactant	$\Delta G_{Z\text{-}E}$	ΔG_{iso}
2	19.7	162.9	6.5	**2**$^{\bullet+}$	31.3	77.2
3	19.6	165.2	7.5	**3**$^{\bullet+}$	33.5	96.9
4	20.6	161.4	8.0	**4**$^{\bullet+}$	30.9	83.8
5	19.5	164.1	7.1	**5**$^{\bullet+}$	31.6	83.8

IX. ELECTROCHEMICAL CHARACTERIZATION

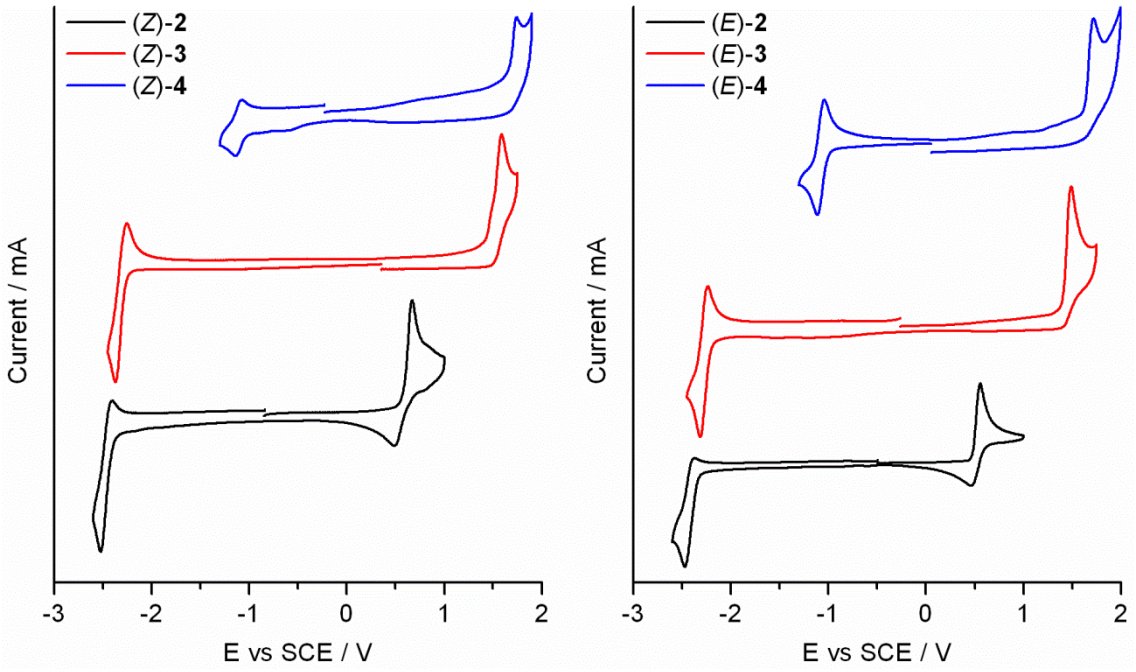

Fig. S10. Cyclic voltammograms of stilbene derivatives **2**, **3** and **4**, where the first reduction and oxidation waves of these compounds can be observed. Measurements were conducted using a glassy carbon electrode as a WE in anhydrous acetonitrile containing 0.1 M of *n*-Bu_4NPF_6 as supporting electrolyte. All the potentials are reported versus an SCE electrode. Scan rate of 0.5 V s^{-1}.

Table S8. Redox potentials for stilbene derivatives **2**, **3**, **4** and **5**.

Compound	E_{red} vs SCE (V)	E_{ox} vs SCE (V)
(*Z*)-**2**	-2.47 [b]	0.58 [a]
(*Z*)-**3**	-2.31 [a]	1.59 [b]
(*Z*)-**4**	-1.11 [a]	1.74 [b]
(*Z*)-**5**	-2.70 [b]	1.13 [b]
(*E*)-**2**	-2.42 [a]	0.51 [a]
(*E*)-**3**	-2.28 [a]	1.49 [b]
(*E*)-**4**	-1.08 [a]	1.72 [b]
(*E*)-**5**	-2.54 [b]	1.10 [b]

[a] Reversible wave. E^0 is given. [b] Irreversible wave. Anodic or cathodic peak potentials are given.

X. REFERENCES

1 M. T. Rojas, R. Königer, J. F. Stoddart and A. E. Kaifer, A. E. *J. Am. Chem. Soc.*, 1995, **117**, 336-343.

2 H. M. Wang and G. Wenz, *Chem. Asian J.*, 2011, **6**, 2390-2399.

3 J. Turkevich, P. C. Stevenson and J. Hillier, *Discuss. Faraday Soc.*, 1951, **11**, 55-75.

4 J. Kimling, M. Maier, B. Okenve, V. Kotaidis, H. Ballot and A. Plech, *J. Phys. Chem. B*, 2006, **110**, 15700-15707.

5 M. A. Uppal, A. Kafizas, M. B. Ewing and I. P. Parkin, *New J. Chem.*, 2010, **34**, 2906-2914.

6 C. S. Weibecker, M. V. Merrit and G. M. Whitesides, *Langmuir*, 1996, **12**, 3763-3772.

7 K. R. Gangwar, V. A. Dhumale, D. Kumari, U. T. Nakate, S. W. Gosavi, R. B. Sharma, S. N. Kale and S. Datar, *Mater. Sci. Eng. C*, 2012, **32**, 2659-2663.

8 E. M. M. del Valle, *Process Biochem.*, 2004, **39**, 1033-1046.

9 J. Liu, W. Ong, E. Román, M. J. Lynn and A. E. Kaifer, *Langmuir*, 2000, **16**, 3000-3002.

10 X. Liu, M. Atwater, J. Wang, and Q. Huo, *Coll. Surf. B Biointerfaces*, 2007, **58**, 3-7.

11 B. D. Wagner and S. Fitzpatrick, *J. Inclus. Phen. Macrocyclic Chem.*, 2000, **38**, 467-478.

12 M. J. Frisch, G. W. Trucks, H. B. Schlegel, G. E. Scuseria, M. A. Robb, J. R. Cheeseman, G. Scalmani, V. Barone, B. Mennucci, G. A. Petersson, et al., *Gaussian Inc Wallingford CT* 2009, Wallingford CT.

13 Y. Zhao and D. G. Truhlar*, J. Phys. Chem. A.*, 2004**, 108**, 6908-6918.

14 R. Ditchfield, W. J. Hehre and J. A. Pople, *J. Chem. Phys.*, 1971, **54**, 724-728.

15 M. Sodupe, J. Bertrán, L. Rodríguez-Santiago and E. J. Baerends, *J. Phys. Chem. A*, 1999, **103**, 166-170.

16 X. Solans-Monfort, V. Branchadell, M. Sodupe, M. Sierka and J. Sauer, *J. Chem. Phys.*, 2004, **121**, 6034-6041.

17 F. Aquilante, T. B. Pedersen, V. Veryazov and R. Lindh, *Wiley Interdiscip. Rev. Comput. Mol. Sci.*, 2013, **3**, 143–149.

18 R. Pou-Amérigo, M. Merchán, I. Nebot-Gil, P. O. Widmark and B. O. Roos, *Theor. Chim. Acta*, 1995, **92**, 149–181.

19 A. Gil, S.Simon, L. Rodríguez-Santiago, J. Bertrán and M. Sodupe, *J. Chem. Theory Comput.*, 2007, **3**, 2210-2220.

20 L. Radom, *J. Phys. Chem. A*, 2007, **111**, 13638-13644.